Rotational isomerization of small carboxylic acids isolated in argon matrices: Tunnelling and quantum yields for the photoinduced processes

Ermelinda M. S. Maçôas,[ab] Leonid Khriachtchev,*[a] Mika Pettersson,†[a] Rui Fausto[b] and Markku Räsänen[a]

[a] Laboratory of Physical Chemistry, University of Helsinki, PO Box 55, FIN-00014 Helsinki, Finland. E-mail: leonid.khriachtchev@helsinki.fi
[b] Department of Chemistry (CQC), University of Coimbra, P-3004-535 Coimbra, Portugal

The quantum yields for internal rotation around the C–O bond induced by excitation of the first overtone of the hydroxyl stretching mode in formic, acetic, and propionic acids isolated in solid Ar are comparatively discussed. The tunnelling kinetics for isomerization from the higher energy arrangement of the carboxylic group (*cis*) to the lower energy arrangement (*trans*) in this series of compounds is also analysed. Finally, the quantum yield for the C_α–C isomerization in propionic acid was investigated and, in contrast with the C–O isomerization, shown to be probably sensitive to the local matrix morphology.

1. Introduction

For a number of molecules, rotational isomerization can be efficiently induced by vibrational excitation of the monomer isolated in low-temperature rare-gas matrices.[1–19] This process occurs when the energy deposited into the initially excited vibrational mode is transferred to the reaction coordinate. The mechanism of energy relaxation in the solid was described as a phonon-assisted intramolecular vibrational energy relaxation (IVR) where the lattice modes provide a thermal bath compensating the energy mismatch between the intramolecular vibrational states.[20,21] The relaxation rates are expected to depend on both the number of phonons involved and temperature of the phonon bath.

The experimental quantum yields for IR-induced rotamerization (rotational isomerization) in rare-gas matrices have been previously reported.[1,11–13] The quantum isomerization yield depends on the proportion of the energy relaxation channels that can deposit energy into the reaction coordinate as well as on the lifetimes of the molecular states involved so that the isomerization is in competition with possible non-reactive energy relaxation channels. The excitation energy, the host, and the nature of the excited mode may affect the IVR process and, consequently, they have been shown to affect the isomerization quantum yields.[11]

For formic (HCOOH, FA) and acetic (CH₃COOH, AA) acids, two stable geometrical arrangements are interconverted by rotation around the C–O axis, the *trans* and *cis* conformers shown in Fig. 1 (C–C–O–H dihedral angles of 180 and 0°, respectively).[5,22] The *trans* form is lower in energy by ≈1400–1800 cm⁻¹ and the *trans* → *cis* isomerization barrier is ≈3900–4400 cm⁻¹.[23–26] These molecules were found mainly in the *trans* conformation in low-temperature matrices.[5,22] The resonant narrowband irradiation of individual vibrational transitions of the matrix isolated molecules in the 2900–7000 cm⁻¹ region induces the *trans* → *cis* conversion.[26–28] Infrared (IR) absorption spectroscopy provides reliable identification of the
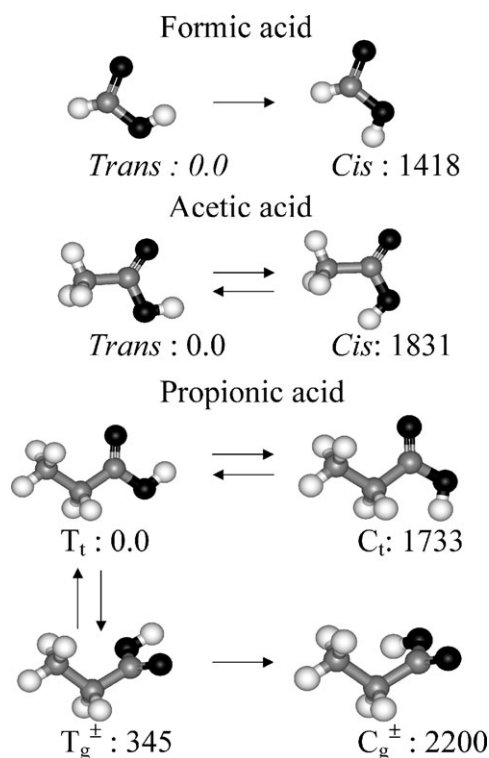
conformers because certain modes are very sensitive to conformation (see Table 1). For both FA and AA, the reverse isomerization from the higher energy conformer (*cis*) to the conformational ground state (*trans*) takes place by tunnelling.[28,29]

Intuitively, isomerization may take place when the energy transferred to the reaction coordinate (C–O torsion, τC–O) is higher than the isomerization barrier. However, for FA and AA, it was shown that this reaction occurs even when the excitation energy deposited into the reaction coordinate is below the isomerization barrier,[26–28] suggesting that tunnelling plays an important role in the photoinduced *trans* → *cis* isomerization process.

The effects of the medium and the nature of the excited state in the *trans* → *cis* isomerization have also been studied.[26,28] For FA, the quantum yield is practically independent of the local environment (matrix site), except when associated with excitation of hindered rotation of the molecule in the matrix.[26] Since AA shows no site structure, the matrix site effect on the quantum yield was not addressed. However, for AA, the isomerization quantum yield upon excitation of the 2νOH mode was shown to be relatively insensitive to the host (Ar, Kr, and Xe).[28] Additionally, excitation of different modes at energies higher than the barrier leads to similar isomerization quantum yields independently of the excited mode (≈20% for FA, and ≈2% for AA).[26,28] Therefore, the nature of the excited mode does not seem to be an important factor to the photoisomerization efficiency in these molecules.

The high efficiency of the isomerization process in FA was connected with the relatively large energy gaps in the vibrational manifold of this molecule, which delays the energy relaxation within the potential well of the initially excited conformer, hence favoring isomerization.[26] It was suggested that the one order of magnitude difference between the quantum yields for FA and AA is due to the methyl group in AA, which increases the number of energy relaxation channels competing with the photoisomerization process.[28] The important role of the methyl group in the photoisomerization process was supported by a large increase of the *trans* → *cis* isomerization quantum yield upon deuteration of the methyl group

† Present address: Department of Chemistry, University of Jyväskylä, PO Box 35, FIN-40014, Finland.

Fig. 1 Conformers of FA, AA and PA. The conformational energies calculated at the MP2/6-311++G(2d,2p) level of theory (in cm^{-1}) are shown. The arrows indicate the observed IR-induced isomerization processes. The IR-induced *cis* → *trans* process for FA has not been studied. The computational *trans* → *cis* barriers are 4096 and 4139 cm^{-1} for FA and AA, respectively. For PA, the T_t → C_t, $T_g^{\pm}$ → $C_g^{\pm}$, T_t → $T_g^{\pm}$ and C_t, → $C_g^{\pm}$ barriers are 4023, 4091, 405 and 559 cm^{-1}, respectively. The barriers are given taking into account the zero point energies.

(by a factor of ≈ 5).[28] For AA, deuteration of the hydroxyl group was shown to reduce the isomerization quantum yield, in contrast to the effect observed for deuteration of the methyl group. In CH$_3$COOD (AA-OD), the *trans* → *cis* quantum yield is almost one order of magnitude lower than in the fully hydrogenated species (AA-OH).[28] Additionally, for CH$_3$COOD and CD$_3$COOD, the *trans* → *cis* isomerization process has a lower quantum yield than the reverse IR-induced *cis* → *trans* process.[28] Similar observations have been reported for HONO isolated in solid Kr.[1]

Propionic acid (CH$_3$CH$_2$COOH, PA) has one additional internal rotational degree of freedom when compared with AA, the internal rotation around the C$_\alpha$–C bond. With respect to the C–O rotation, PA is similar to FA and AA. Recently, the four PA conformers built up from combinations of the stable C–O (*trans* and *cis*) and C$_\alpha$–C (*trans* and *gauche*, with C–C–C–O dihedral angles of 180° and $\pm \approx 75°$, respectively) arrangements have been identified using IR-induced isomerization in solid

Ar.[30] The structure and energetics of the PA conformers predicted by *ab initio* calculations are shown in Fig. 1 and the characteristic vibrational frequencies for the T_t and C_t forms are given in Table 1. The IR-induced isomerization processes identified for PA isolated in solid Ar are also indicated in Fig. 1. The quantification of the isomerization quantum yields for the C–O and C$_\alpha$–C rotations in propionic acid gives further insight into factors affecting the rotamerization process.

In the present work, we compare IR-induced rotational isomerization and tunnelling processes for formic, acetic and propionic acids in solid Ar. The data for FA and AA were previously reported,[26,28] and the results for PA are described here for the first time. By analysing comparatively the data obtained for all these species, it is possible to test previous interpretations and understand better how the vibrational density of states, deuteration of the hydroxyl group, and the matrix surrounding affect the isomerization process. It is not a purpose of this article to describe in detail spectroscopic identification and properties of the four PA conformers, and we present here only limited spectroscopic data (see Table 1).

2. Experimental details and methodology

The gaseous samples were prepared by mixing the carboxylic acids ($>99\%$), degassed by several freeze–pump–thaw cycles, with high purity argon (99.9999%), in the 1 : 500 to 1 : 2000 ratio. Hydroxyl-deuterated PA was obtained by H/D exchange on the inner surface of the sample container and the deposition line saturated with D$_2$O. The gaseous mixtures were deposited onto a CsI substrate kept at 15 K in a closed cycle helium cryostat (APD, DE 202A) and subsequently cooled down to 8 K. The IR absorption spectra (7900–400 cm^{-1}) were measured with a Nicolet SX-60 FTIR spectrometer. A liquid-nitrogen cooled MCT detector and a Ge/KBr beamsplitter were used to record the mid-IR absorption spectra with spectral resolution from 0.25 to 1.0 cm^{-1}. A liquid-nitrogen-cooled InSb detector and a quartz beamsplitter were used to record the near-IR (NIR) absorption spectra with spectral resolution of 0.5 cm^{-1}. Typically 100 to 500 interferograms were co-added.

Tunable pulsed IR radiation provided by an optical parametric oscillator (Continuum, OPO Sunlite with IR extension) was used to excite vibrations of the studied molecules. The pulse duration was ≈ 5 ns, the spectral linewidth ≈ 0.1 cm^{-1} and the repetition rate 10 Hz. The pulse energy of the OPO in the 7000–5000 cm^{-1} spectral region was ≈ 0.5 mJ. The OPO radiation frequency was measured with a Burleigh WA-4500 wavemeter providing an absolute accuracy better than 1 cm^{-1} for the IR pumping radiation. The pumping beam was quasi-collinear with the spectrometer beam, and interference filters (transmitting in the 3650–3400 cm^{-1} or 3300–1100 cm^{-1} regions) were placed in front of the detector to prevent its exposure to the pumping radiation while recording spectra during irradiation.

Table 1 Experimental characteristic frequencies for the conformers of FA, AA and PA exhibiting the *trans* or *cis* arrangements of the carboxylic group (C–C–O–H dihedral angle of 180° and 0°, respectively)[30,32,33]

	trans		*cis*			
	νOH(D)	νC=O	νOH(D)	νC=O	$[\Delta\nu\text{OH(D)}]_{cis-trans}$	$[\Delta\nu\text{C=O}]_{cis-trans}$
HCOOH	3550	1768	3617	1808	+67	+40
DCOOH	3550	1761	3616	1777	+66	+16
CH$_3$COOH	3564	1779	3623	1807	+59	+28
CD$_3$COOH	3564	1777	—	1798	—	+21
CH$_3$COOD	2629	1770	2674	1800	+45	+30
CD$_3$COOD	2630	1765	2673	1794	+43	+29
CH$_3$CH$_2$COOH	3567	1776	—	1802	—	+26
CH$_3$CH$_2$COOD	2630	1766	2674	1797	+44	+31

The *ab initio* calculations were performed using the GAUS-SIAN98 program at the MP2/6-311++G(2d,2p) level of approximation.[31]

The quantum yields of the rotamerization processes, $\phi(i)$, were extracted from the following equation:

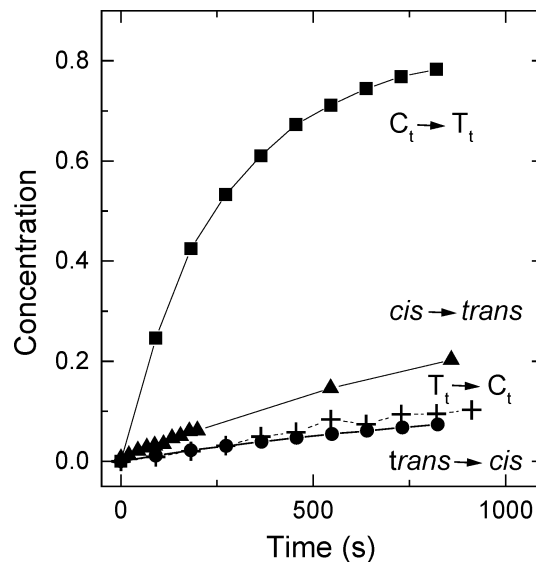$$\phi(i) = \frac{k_p(\nu)}{\sigma^i(\nu)I(\nu)} \quad (1)$$

where $k_p(\nu)$ (in s^{-1}) is the averaged isomerization rate upon pumping at the frequency ν, $\sigma^i(\nu)$ (in cm^2) is the absorption cross-section of the mode i at the excitation frequency, and I (in s^{-1} cm^{-2}) is the averaged photon intensity of the pumping beam. The cross-section is obtained using the measured IR absorption at the excitation frequency, the estimated concentration of molecules in the excited matrix site, and the matrix thickness. For PA, the absorption cross-sections at the frequency used to excite the 2νOH and 2νOD modes of T_t are $\approx 3.6 \times 10^{-20}$ cm^2, and $(3.2–4.1) \times 10^{-20}$ cm^2 (depending on the matrix site), respectively. For the 2νOH mode, the cross-sections for PA is smaller than the value obtained for the same mode of FA and AA by a factor of ≈ 5. In the case of the 2νOD mode, the σ values are $\approx 2–3$ times smaller for PA than for AA (the value for FA has not been reported). These values correspond to the maximum of the absorption bands, and the smaller values for PA reflect essentially the fact that these bands are broader for PA than for FA and AA. The absorption cross-section of the 2νOD mode of the C_t conformer could not be measured directly due to its low concentration in the matrix. It was assumed that the absorption cross-section of the 2νOD mode of C_t is similar to the value for T_t by analogy with the data for *cis* and *trans* AA-OD.

Two methodologies have been applied to determine the pumping rate, k_p in eqn. (1). The most straightforward approach employs the IR-induced formation kinetics of the conformers. This approach was previously applied to the estimation of isomerization quantum yields for AA-OD.[28] In the present work, the PA concentration was followed by measuring the integrated absorption of the νOH or νOD modes upon IR pumping. To minimize errors on the determination of the pumping rates caused by reverse isomerization processes, only the points obtained during the first minutes of irradiation were considered. As an example, Fig. 2 shows the IR-induced formation kinetics for two conformers of AA-OD (*trans* and *cis*) and PA-OD (T_t and C_t).

The kinetics-based methodology could be used when the reverse isomerization was relatively slow. This is not the case for the $T_t \rightarrow C_t$ process in PA-OH where the backreaction taking place by tunnelling is too fast to follow reliably the pumping kinetics. The C_t concentration saturates very quickly at a quite low level upon pumping the 2νOH mode of the T_t form. This stationary state is established as a result of the interplay between photoinduced generation of the C_t conformer and its depletion due to the $C_t \rightarrow T_t$ tunnelling. In this case, a way to obtain the pumping rate follows the procedure previously reported for the hydrogenated isotopologues of FA and AA.[26,28] At the equilibrium the pumping and tunnelling rates are equal, then:

$$k_p(\nu)[T_t]_{eq} = k_t(T)[C_t]_{eq} \quad (2)$$

where $k_t(T)$ is the tunnelling rate coefficient at the temperature T. Hence, the pumping rate can be determined from the measured $C_t \rightarrow T_t$ tunnelling rate and the ratio of the T_t and C_t equilibrium concentrations. The tunnelling rate is extracted from the decay kinetics of the C_t conformer (see Fig. 3), which is obtained by recording IR absorption spectra every 10 s co-adding only 5 interferograms for each spectrum. The C_t/T_t concentration ratio at the equilibrium can be extracted from the changes in integrated absorptions upon pumping as described previously for FA.[26] The most important error of the
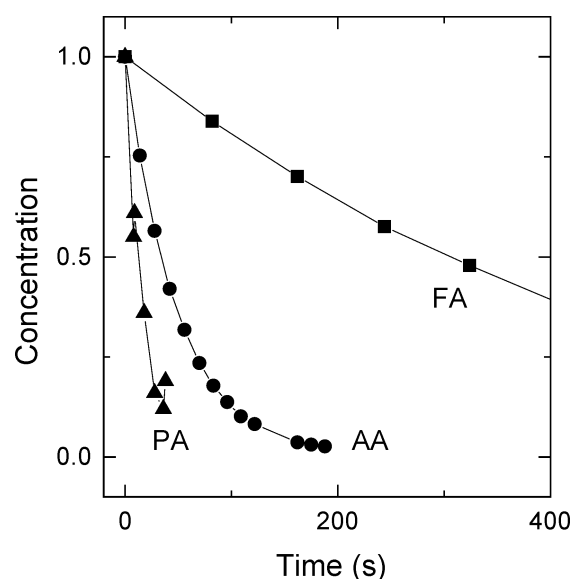

Fig. 2 Pumping kinetics measured for hydroxyl-deuterated AA and PA. The concentrations of the photoproducts are normalised by the initial concentrations of the pumped conformer. The pumping rates are extracted from a linear fit of the beginning of the kinetics curves. For AA, the pumping rates for the *trans* → *cis* (●) and *cis* → *trans* (▲) processes differ by a factor of ≈ 3, whereas for PA, the rates for the $T_t \rightarrow C_t$ (+) and $C_t \rightarrow T_t$ (■) processes differ by a factor of ≈ 25. The lines are merely guides. The T_t and C_t conformers in the LF site were pumped.

isomerization quantum yield obtained from eqn. (1) can come from the estimated proportion of molecules isolated in various matrix sites, independently of the method used to obtain k_p. It was assumed here that the absorption intensity is independent of the matrix site.

As another approach, the quantum yield is a ratio of the number of molecules that undergo isomerization (N_{iso}) to the number of absorbed photons (N_{abs}):

$$\phi(i) = \frac{N_{iso}}{N_{abs}} \quad (3)$$

The value of N_{abs} per unit time is estimated from the absorbance at the excitation frequency, A_{exc}, the intensity of the

Fig. 3 Tunnelling kinetics for the conversion from the higher energy (*cis*) to the lower energy (*trans*) arrangement of the carboxylic group of fully hydrogenated FA (■, *cis* → *trans*), AA (●, *cis* → *trans*) and PA (▲, $C_t \rightarrow T_t$) measured in solid Ar at 8 K. The lines are merely guides. The data are normalised by the initial concentrations.

incoming beam (in $cm^{-2}\,s^{-1}$), I_0, and the irradiated area, S, as follows:

$$N_{abs} = (1-10^{-A_{exc}})I_0 S \qquad (4)$$

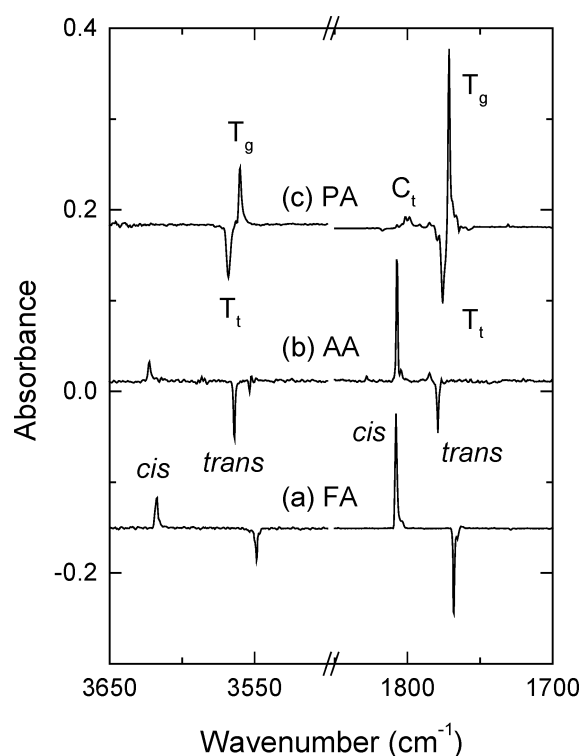The number of isomerization events per unit time is calculated as follows:

$$N_{iso} = \frac{\left(\frac{\Delta A}{A_0}\right)n}{\Delta t} \qquad (5)$$

where Δt is the irradiation time, n is the total number of molecules of the excited conformer, A_0 and ΔA are the initial integrated absorption and the change in integrated absorption for a given vibrational mode of the pumped conformer. ΔA is related to isomerization induced in a specific site, and it is measured directly from the difference IR absorption spectra. Note that ΔA for a given pumping time can be estimated only if the pumping kinetics is followed in real time, and N_{abs} can only be estimated if the NIR spectrum is measured before pumping.

3. Results and discussion

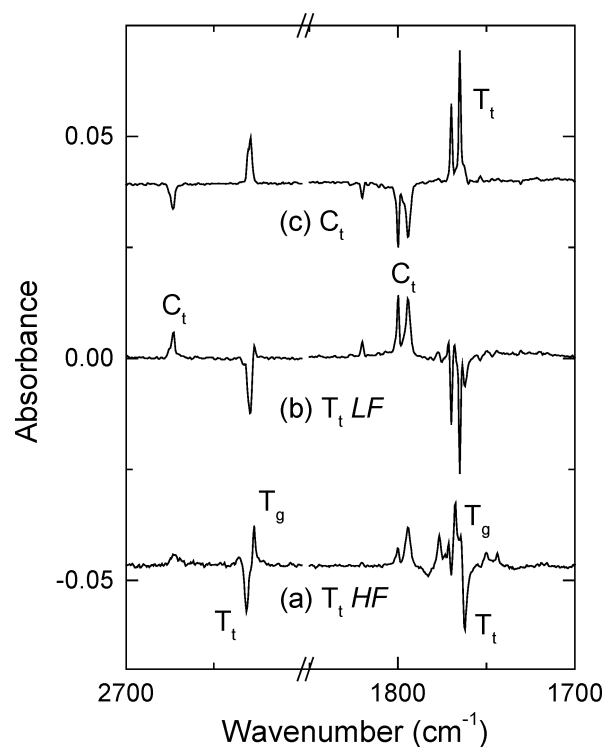### 3.1. Identification of the conformers by IR absorption spectroscopy

For various isotopologues of FA and AA, excitation of the $2\nu OH(D)$ modes is efficient in promoting isomerization around the C–O bond (C–O isomerization).[26,28] The IR-induced changes in the $\nu OH(D)$ and $\nu C=O$ spectral region can be used to identify the conformers involved because they are very sensitive to the conformation of the carboxylic group (see Table 1). For FA and AA, the $\nu OH(D)$ and $\nu C=O$ modes appear blue-shifted by 40–60, and 20–40 cm^{-1}, respectively, in the *cis* as compared with the *trans* conformer.[32,33] For FA and AA, the traces (a) and (b) in Fig. 4 show the difference IR spectra where the increasing bands of the *cis* forms are clearly blue-shifted from the decreasing bands of the *trans* forms.

Similarly to FA and AA, PA is found after deposition in the ground conformational state, the T_t form (see Table 1 for the characteristic vibrational frequencies).[30] Excitation of the $2\nu OH(D)$ mode of T_t induces the C–O and C_α–C isomerizations, which lead to the production of the C_t and $T_g^\pm$ conformers, respectively. The bands of C_t are most clearly observed in the spectra recorded *under* pumping of T_t because its concentration quickly decreases when the excitation of T_t is interrupted, even at 8 K (see Fig. 3). The C_t form converts back to the most stable T_t form by tunnelling, in analogy with the *cis* → *trans* tunnelling observed for FA and AA.[28,29] For PA, trace (c) in Fig. 4 shows a difference spectrum obtained under excitation of the $2\nu OH$ mode of T_t. In this spectrum the emerging bands slightly red-shifted from those of T_t, in both the νOH and $\nu C=O$ spectral regions are assigned to the $T_g^\pm$ form resulted from the C_α–C internal rotation. These small shifts agree with a predictable small effect of the backbone conformation on the vibrational modes localized in the carboxylic group. The weaker band rising at ≈ 1800 cm^{-1} is assigned to the $\nu C=O$ mode of C_t, which is produced from T_t by internal rotation along the C–O bond. The $\nu C=O$ band of C_t shows the expected large blue-shift from that of T_t. The νOH band is not observed for C_t most probably due to its low intensity and also due to the fact that it is expected to appear at ≈ 3630 cm^{-1}, which is very close to the cut-off of the filter used to record the spectrum under irradiation.

As an important fingerprint of tunnelling, substitution of the tunnelling particle by a heavier isotope decreases the reaction rate significantly. Consequently, deuteration of the hydroxyl group of PA facilitates identification of the C_t conformer produced upon excitation of the ground-state T_t form. Spectra (a) and (b) in Fig. 5 show the results of conformational isomerization of PA-OD induced by excitation of the T_t form in two different matrix sites at 5175 and 5170 cm^{-1} (hereafter denoted as HF and LF, respectively). Similarly to PA-OH, the

Fig. 4 Difference IR absorption spectra showing the spectral changes produced by excitation at the $2\nu OH$ frequencies of the ground state conformers of fully hydrogenated FA (a), AA (b) and PA (c). The difference spectra are obtained as spectra measured *after* pumping minus spectra measured *before* pumping for FA and AA, and a spectrum *during* pumping minus a spectrum *before* pumping for PA.

Fig. 5 Difference IR absorption spectra of PA-OD showing the conformational changes induced by excitation of the $2\nu OD$ modes of (a) T_t in the HF site (40 min), (b) T_t in the LF site (40 min), and (c) C_t in the LF matrix site (15 min). Traces (a) and (b) show the increasing of C_t and $T_g^\pm$ bands produced from T_t *via* the C–O and C_α–C isomerization and trace (c) shows the increasing of T_t bands produced from C_t due to the C–O isomerization. The pumped species are marked.

increasing bands in the two difference spectra, which appear considerably blue-shifted from the T_t bands, are assigned to the C_t conformer while the less shifted bands are due to the $T_g^{\pm}$ conformer. In agreement with our calculations, the $T_g^{\pm}$ bands are close to the T_t bands, and they appear slightly red-shifted or blue-shifted depending on the matrix site.

Additionally, the C_t form is much more stable for PA-OD than for PA-OH, which allowed us to perform pumping experiments with the C_t conformer of PA-OD. As seen in plot (c) of Fig. 5, excitation of the 2νOD of the C_t molecules previously produced in the LF site leads to the $C_t \rightarrow T_t$ isomerization.

3.2. Tunnelling rate for the C–O isomerization

For PA-OH, the $C_t \rightarrow T_t$ tunnelling is faster than the analogous $cis \rightarrow trans$ tunnelling for FA and AA (Fig. 4).[28,29] The tunnelling rate for the C–O isomerization observed for fully hydrogenated FA, AA and PA ($k_t \approx 2 \times 10^{-3}$, 2×10^{-2}, and 5×10^{-2} s^{-1}, respectively) correlates inversely with the barrier height for the isomerization, i.e., the higher barriers reasonably correspond to slower tunnelling rates. The $cis \rightarrow trans$ barrier heights calculated in this study at the MP2/6-311++G(2d,2p) level of theory for FA, AA and PA, are 2676, 2308 and 2290 cm^{-1}, respectively. The tunnelling rate for FA is one order of magnitude slower than for AA, thus, reflecting the considerably higher barrier for the $cis \rightarrow trans$ conversion in FA as compared with AA (the computational difference between the barriers ≈ 370 cm^{-1}). For AA and PA, the calculated barrier heights differ only by ≈ 20 cm^{-1} and the tunnelling rates are closer to each other. The known solvation effect can change to some extent the relative energetics and the barriers, as it was discussed elsewhere,[29] however, this energy change should be similar for the species under study.

For FA, deuteration of the hydroxyl group decreases the $cis \rightarrow trans$ tunnelling rate by a factor of $\approx 3 \times 10^3$ (from 2×10^{-3} to 7×10^{-7} s^{-1}). For AA and PA, deuteration of the hydroxyl group decreases the tunnelling rate by even larger factors of 3×10^4 and 6×10^4 (from 2×10^{-2} to 7×10^{-7} s^{-1} for AA and from 5×10^{-2} to 8×10^{-7} s^{-1} for PA). It is remarkable that the effect of hydroxyl deuteration is higher for lower isomerization barriers. This effect is in contradiction with the expected trend for the penetration probability calculated according to the semi-classical WKB approximation.[34] It is probable that the tunnelling rate depends essentially on additional factors like the nature and distribution of the vibrational energy levels involved in the tunnelling process as pointed out in our previous studies on FA and AA.[28,29] Our present results support the previously suggested model. It should be also mentioned that the extraction of very small decay rates is complicated and produces a relatively large experimental error.

3.3. IR induced trans → cis C–O isomerization in the fully hydrogenated species

For the three molecules under study, the quantum yields obtained for the $trans \rightarrow cis$ C–O isomerization induced by excitation of the 2νOH mode of the ground state conformer are shown in Table 2. The strong decrease in the quantum yield from FA (10–20%)[26] to AA ($\approx 2\%$)[28] was previously connected with the low-barrier methyl rotor in the latter molecule. The low-frequency modes of the methyl rotor are coupled with the initially excited mode or/and with intermediate vibrational modes participating in the energy relaxation, enhancing non-reactive relaxation channels.[35] Vibrations with large amplitudes such as τC–O and τC–CH$_3$ are usually very anharmonic and strong coupling between the two internal rotors in AA can be expected.

PA has one additional internal rotational degree of freedom when compared with AA, the C_α–C torsion (τC$_\alpha$–C). This

Table 2 Quantum yields for C–O isomerization induced by excitation of the 2νOH/2νOD modes of the fully hydrogenated and hydroxyl-deuterated FA,[26] AA,[28] and PA

C–O isomerization quantum yields[a]	FA[b]	AA	PA
2νOH	1.7×10^{-1} (s2)	2.2×10^{-2}	1.4×10^{-2}
trans → cis	7×10^{-2} (s1)		
2νOD			
trans → cis	—	3.6×10^{-3}	3.2×10^{-3} (HF)
2νOD			5.0×10^{-3} (LF)
cis → trans	—	1.2×10^{-2}	1.4×10^{-1}

[a] The quantum yields have been estimated by eqn. (1), the estimated error is $\pm 50\%$. For PA, the trans and cis form correspond to T_t and C_t, respectively. The two entries for FA and PA are associated with excitation of different sites (s1 and s2 in FA, and HF and LF in PA).[26,30] [b] No kinetic data available for excitation of 2νOD.

mode has a low vibrational frequency and it can contribute to the energy relaxation process in PA similarly to the τC–CH$_3$ mode. In fact, the computational frequency for the τC$_\alpha$–C mode in T_t is 57 cm^{-1}, i.e. very close to the value of the Debye frequency for solid Ar (≈ 60 cm^{-1}),[36] which can favour energy transfer between lattice vibrations and molecular modes. Indeed, in addition to the C–O internal rotation, excitation of the 2νOH mode of PA induces the C_α–C internal rotation indicating that the excitation energy is channelled efficiently into the low-frequency C_α–C torsional mode. The quantum yield for the C_α–C isomerization ($T_t \rightarrow T_g^{\pm}$) is 1.4%. Despite of this additional reaction channel, competing with the C–O isomerization, the quantum yield for the C–O isomerization in PA (1.4%) is similar to the value for AA within our experimental error (see Table 2). A more quantitative analysis of the isomerization process should be based on the vibrational patterns in the overtone and combination spectral region derived from the precise anharmonic analysis. It is difficult to specify the involved relaxation channels for a relatively complicated system like PA with unknown anharmonic coupling between modes. In any case, the balance between the efficiency of the non-reactive and reactive channels is not changed significantly in PA as compared with AA. With respect to the C–O isomerization, the participation of the CH$_3$ group seems to be comparable to the effect of the CH$_3$CH$_2$ group. Thus, relatively large isomerization quantum yields may be expected for related molecules with longer carbon chains, which is an interesting direction of research.

3.4. IR-induced trans → cis and cis → trans C–O isomerization in the OD-species

The $T_t \rightarrow C_t$ isomerization quantum yield for PA-OD (0.32–0.50%) is similar to the value estimated for AA-OD (0.4%). For both AA and PA, deuteration of the hydroxyl group decreases significantly the C–O isomerization quantum yield. This phenomenon should not be correlated with the lower excitation energy upon pumping the 2νOD mode (≈ 5100 cm^{-1}) when compared to the 2νOH mode (≈ 6900 cm^{-1}) or with the change of the zero point vibrational energy. Indeed, it was shown for FA and AA that the C–O isomerization quantum yields are nearly insensitive to the excitation energy as long as the energy is above the isomerization barrier.[26,28] Our explanation for the deuteration effect observed in AA was based on the participation of higher order couplings between the τC–O and the intermediate states involved in the IVR process for the OD species in comparison with the OH species. The higher order couplings for the OD species are due to a deuteration-induced decrease of the τC–O frequency, and therefore, at similar energies the τC–O mode is at a higher excited state in the OD species. This reduces the probability of

energy transfer into the reaction coordinate for the deuterated species.[28] In this study, we also observed a decrease of the $T_t \rightarrow T_g^\pm$ quantum yield for PA-OD ($<0.2\%$) compared with PA-OH (1.4%), indicating a significant effect even when the corresponding mode is not influenced much by deuteration. In order to justify this observation, we can speculate that the deuteration can decrease the coupling of the pumped mode [2νOH(D)] with the reaction coordinate.

In the case of PA-OD, the estimated quantum yield is much larger for the reverse $C_t \rightarrow T_t$ conversion (14%) than for the $T_t \rightarrow C_t$ conversion (0.32–0.50%). This constitutes already the third reported observation pointing to the same direction, taking into account similar effects observed for the *cis* → *trans* isomerization in the AA-OD (Table 2)[28] and HONO.[1] For HONO, the quantum yield higher by a factor of 7 was found for the IR-induced conversion of the *cis* conformer (H–O–N=O dihedral angle of 0°) into the *trans* form (H–O–N=O dihedral angle of 180°) when compared with the *trans* → *cis* process.[1] Although the *cis* → *trans* energy barriers in AA and PA are lower than the *trans* → *cis* barriers, this fact is unable to fully justify the observed trend for two reasons: (1) the difference in the *cis* → *trans* and *trans* → *cis* barriers for HONO is very small (130 cm^{-1}) and (2) the quantum yields for FA and AA are quite independent of the excitation energy as long as the excited vibrational mode is above the isomerization barrier.[1,26,28] In the case of HONO, it was suggested that kinetic or potential couplings between the excited vibrations and nearly resonant vibrational states could be responsible for the more efficient energy transfer from the excited states to the reaction coordinate upon excitation of the *cis* isomer.[37,38] These factors may also be relevant for the carboxylic acids studied here.

3.5. Site-selective isomerization of PA-OD

Fig. 5 presents the result of irradiation for the hydroxyl-deuterated T_t conformer at two slightly different frequencies (5175 and 5170 cm^{-1}). The pumping at different frequencies excites molecules in different local matrix morphologies (matrix sites). It is seen that the ratio of the $T_t \rightarrow C_t$ and $T_t \rightarrow T_g^\pm$ reaction channels upon excitation of the 2νOD of T_t depends on the matrix site, in particular, excitation of the HF site is more efficient in promoting the C_α–C internal rotation than excitation of the LF site. The quantum yields obtained for the C_α–C isomerization process differ by a factor of ≈ 4 (0.16 and 0.042% for HF and LF excitation, respectively) suggesting the site selectivity of this reaction channel (Table 3). On the other hand, the quantum yields for the C–O isomerization upon pumping the HF and LF sites are similar within our experimental error (0.32 and 0.50% for HF and LF excitation, respectively). The latter result is similar to the data on FA where no reliable site dependence of the C–O isomerization quantum yield has been observed.[26] For PA, we can compare the isomerization quantum yields for the two isomerization processes for molecules isolated in the same matrix site. The C–O isomerization is the preferred reaction channel for pumping of the LF site (5170 cm^{-1}), and the C–O isomerization quantum yield is higher than that associated with the C_α–C process by more than one order of magnitude. For pumping of the HF site (5175 cm^{-1}), the two photoprocesses are nearly as efficient. The quantum yields given in Table 3 were estimated by the two different methods described earlier [eqns. (1) and (3)], and the obtained values are rather independent of the method used.

The site dependence of the quantum yields is possibly contributed by restrictions to the C_α–C internal rotation imposed by the matrix cage. Indeed, the C_α–C isomerization involves rotation of heavy atoms, and hence it is associated with a relatively large reaction volume compared with the C–O isomerization, which deals essentially with motion of the light

Table 3 Quantum yields for C–O and C_α–C isomerization induced by excitation of the 2νOD modes of PA-OD isolated in two matrix sites

Quantum yields^a/10^{-3}	HF site	LF site
$T_t \rightarrow C_t$ (C–O)	3.2 (3.5)	5.0 (5.5)
$T_t \rightarrow T_g^\pm$ (C_α–C)	1.6 (1.7)	0.42 (0.58)

^{a} The values obtained from eqn. (1) are shown outside the parentheses and the results obtained from eqn. (3) are shown in parentheses. An error of $\pm 50\%$ is estimated.

hydroxylic hydrogen atom. These arguments were used previously to explain the lack of NIR induced isomerization in fumaric acid.[39] However, in the case of PA, it was observed that the $T_g^\pm \rightarrow T_t$ dark process is thermally activated, and it is in minute timescale at 15 K. It follows that the corresponding barrier is quite low, which is consistent with the computational value of ≈ 60 cm^{-1}. This suggests that the $T_t \rightarrow T_g^\pm$ barrier should be relatively low as well (computationally ≈ 400 cm^{-1}), which does not support cage restrictions. As another explanation, some specific energy relaxation channels can contribute to the site selectivity of the process. In this image, the coupling of $\tau(C_\alpha$–C) with the lattice vibrations may be important. It should be also noted that the estimation of the C_α–C quantum yields can be influenced by the overlap of the 2νOD bands of the $T_g^\pm$ and T_t conformers. Inspection of the band profiles associated with the two sites leads to the conclusion that this overlap may occur only for the LF site, which, in principle, can contribute to the site selectivity of the C_α–C process, decreasing the $T_g^\pm$ concentration for the LF pumping.

Another observation features unexpected energy redistribution in the molecule. The excitation of the 2νOD of C_t, which is mainly isolated in the LF site (C_α–C resistant site), induced exclusively rotation around the C–O axis leading to production of T_t, and no C_α–C isomerization ($C_g^\pm$) could be detected. In fact, only the bands of T_t increase under vibrational excitation of C_t [spectrum (c) in Fig. 5]. This observation is remarkable since the computational $C_t \rightarrow T_t$ barrier is larger than the $C_t \rightarrow C_g^\pm$ barrier by ≈ 1700 cm^{-1} so that the opposite trend could be expected. This observation may be relevant to the site selectivity of the isomerization process because the opposite $T_t \rightarrow C_t$ process in this site also dominated over the C_α–C isomerization.

4. Conclusions

The quantum yields for the C–O isomerization induced by excitation of the first overtone of the hydroxyl stretching vibration have been estimated for PA isolated in solid Ar, and compared with the corresponding data on FA and AA.[26–28] The *cis* → *trans* tunnelling kinetics was also comparatively analysed. We observed the following trends:

(1) For the fully hydrogenated species, the C–O isomerization quantum yields for PA and AA are one order of magnitude smaller than the value for FA, which is probably caused by a smaller vibrational density of states in the latter molecule. On the other hand, the quantum yields for PA and AA are remarkably similar despite the higher vibrational density of states in PA, thus, indicating a 'saturation' effect.

(2) Similarly to AA, deuteration of the hydroxyl group of PA decreases significantly the C–O isomerization quantum yield. The explanation for the observed deuteration effect relies on the lower probability for energy transfer to the reaction coordinate in the deuterated species due to less efficient couplings between the initially excited vibrational mode and the τC–O reactive mode.

(3) In the case of PA-OD, the C–O and C_α–C isomerization quantum yields were estimated for excitation of molecules isolated in two matrix sites. A site-selective quantum yield

was tentatively observed for the C_α–C isomerization whereas no significant site effect is found for the C–O isomerization. The latter fact corresponds to the data obtained for AA and FA.[26,28]

(4) For AA-OD and PA-OD, the C–O isomerization starting from the higher energy arrangement of the carboxylic group ($cis \rightarrow trans$ in AA; and $C_t \rightarrow T_t$ in PA) was shown to be more efficient than the reverse process. This corresponds to the previous observations in HONO,[1] and it is possibly explained by specific kinetic or potential couplings favouring the $cis \rightarrow trans$ conversion.[37,38]

(5) For the fully hydrogenated species, the measured tunnelling rates correlate inversely with the computational isomerization barrier. Surprisingly, the deuteration effect (decrease of tunnelling rate by several orders of magnitude) is stronger for the lower isomerization barriers (AA and PA). This fact features the influence on the tunnelling mechanism of factors like distribution and nature of the vibrational energy levels involved in the process as proposed earlier for FA.[29]

The results obtained for PA support the conclusions derived previously for FA and AA and increase their confidence. However, understanding of a number of processes is still lacking, which suggests further studies in this field.

Acknowledgements

References

1 L. Khriachtchev, J. Lundell, E. Isoniemi and M. Räsänen, *J. Chem. Phys.*, 2000, **113**, 4265.
2 A. J. Barnes, *J. Mol. Struct.*, 1984, **113**, 161.
3 M. Räsänen, H. Kunttu and J. Murto, *Laser Chem.*, 1988, **9**, 123.
4 S. Sander, H. Willner, L. Khriachtchev, M. Pettersson, M. Räsänen and E. L. Varetti, *J. Mol. Spectrosc.*, 2000, **203**, 145.
5 M. Pettersson, J. Lundell, L. Khriachtchev and M. Räsänen, *J. Am. Chem. Soc.*, 1997, **119**, 11715.
6 E. M. S. Maçôas, L. Khriachtchev, M. Pettersson, J. Lundell, R. Fausto and M. Räsänen, *Vib. Spectrosc.*, 2004, **34**, 73.
7 H. H. Gunthard, *J. Mol. Struct.*, 1984, **113**, 141.
8 R. N. Perutz, *Chem. Rev.*, 1985, **85**, 77.
9 T. Lotta, J. Murto, M. Räsänen and A. Aspiala, *J. Mol. Struct.*, 1984, **114**, 333.
10 S. Kudoh, M. Takayanagi, M. Nakata, T. Ishibashi and M. Tasumi, *J. Mol. Struct.*, 1999, **479**, 41.
11 A. K. Knudsen and G. C. Pimentel, *J. Phys. Chem.*, 1991, **95**, 2823.
12 W. F. Hoffman and J. S. Shirk, *Chem. Phys.*, 1983, **78**, 331.
13 P. Roubin, S. Varin, P. Verlaque, S. Coussan, J. M. Berset, J. M. Ortega, A. Peremans and W. Q. Zheng, *J. Chem. Phys.*, 1997, **107**, 7800.
14 M. Poliakoff and J. J. Turner, in *Chemical and biochemical applications of lasers*, ed. C. B. Moore, Academic, New York, 1980.
15 H. Frei and G. C. Pimentel, *Annu. Rev. Phys. Chem.*, 1985, **36**, 491.
16 H. Frei and G. C. Pimentel, in *Chemistry and Physics of Matrix-Isolated Species*, ed. L. Andrews and M. Moskovits, Elsevier, Amsterdam, 1989.
17 M. Räsänen and V. E. Bondybey, *Chem. Phys. Lett.*, 1984, **111**, 515.
18 M. Räsänen and V. E. Bondybey, *J. Chem. Phys.*, 1985, **82**, 4718.
19 M. Räsänen, J. Murto and V. E. Bondybey, *J. Phys. Chem.*, 1985, **89**, 3967.
20 V. E. Bondybey, *Annu. Rev. Phys. Chem.*, 1984, **35**, 591.
21 F. Legay, in *Chemical and Biochemical Applications of Lasers*, ed. C. B. Moore, Academic, New York, 1977.
22 E. M. S. Maçôas, L. Khriachtchev, M. Pettersson, R. Fausto and M. Räsänen, *J. Am Chem. Soc.*, 2003, **125**, 16188.
23 J. D. Goddard, Y. Yamaguchi and H. F. Schaefer, *J. Chem. Phys.*, 1992, **96**, 1158.
24 W. H. Hocking, *Z. Naturforsch. A*, 1976, **31**, 1113.
25 M. L. Senent, *Mol. Phys.*, 2001, **99**, 1311.
26 E. M. S. Maçôas, L. Khriachtchev, M. Pettersson, J. Juselius, R. Fausto and M. Räsänen, *J. Chem. Phys.*, 2003, **119**, 11765.
27 M. Pettersson, E. M. S. Maçôas, L. Khriachtchev, R. Fausto and M. Räsänen, *J. Am. Chem. Soc.*, 2003, **125**, 4058.
28 E. M. S. Maçôas, L. Khriachtchev, M. Pettersson, R. Fausto and M. Räsänen, *J. Chem. Phys.*, 2004, **121**, 1331.
29 M. Pettersson, E. M. S. Maçôas, L. Khriachtchev, J. Lundell, R. Fausto and M. Räsänen, *J. Chem. Phys.*, 2002, **117**, 9095.
30 E. M. S. Maçôas, L. Khriachtchev, M. Pettersson, R. Fausto and M. Räsänen, unpublished.
31 M. J. T. Frisch, G. W. Schlegel, H. B. Scuseria, G. E. Robb, M. A. Cheeseman, J. R. Zakrzewski, V. G. Montgomery, J. A. Stratmann, R. E. Burant, J. C. Dapprich, S. Millam, J. M. Daniels, A. D. Kudin, K. N. Strain, M. C. Farkas, O. Tomasi, J. Barone, V. Cossi, M. Cammi, M. Mennucci, B. Pomelli, C. Adamo, C. Clifford, S. Ochterski, J. Petersson, G. A. Ayala, P. Y. Cui, Q. Morokuma, K. Malick, D. K. Rabuck, A. D. Raghavachari, K. Foresman, J. B. Cioslowski, J. Ortiz, J. V. Baboul, A. G. Stefanov, B. B. Liu, G. Liashenko, A. Piskorz, P. Komaromi, I. Gomperts, R. Martin, R. L. Fox, D. J. Keith, T. Al-Laham, M. A. Peng, C. Y. Nanayakkara, A. Gonzalez, C. Challacombe, M. Gill, P. M. W. Johnson, B. G. Chen, W. Wong, M. W. Andres, J. L. Head-Gordon, M. Replogle and E. S. Pople, *GAUSSIAN 98 (Revision A. 9)*, Gaussian, Inc., Pittsburgh, PA, 1998.
32 E. M. S. Maçôas, J. Lundell, M. Pettersson, L. Khriachtchev, R. Fausto and M. Räsänen, *J. Mol. Spectrosc.*, 2003, **219**, 70.
33 E. M. S. Maçôas, L. Khriachtchev, R. Fausto and M. Räsänen, *J. Phys. Chem. A*, 2004, **108**, 3380.
34 R. P. Bell, *The tunnel effect in chemistry*, Chapman and Hall, New York, 1980.
35 A. McIlroy and D. J. Nesbitt, *J. Chem. Phys.*, 1994, **101**, 3421.
36 H. J. Jodl, in *Chemistry and Physics of Matrix-Isolated Species*, ed. L. Andrews and M. Moskovits, Elsevier, Amsterdam, 1989.
37 Y. Guan, G. C. Lynch and D. L. Thompson, *J. Chem. Phys.*, 1987, **87**, 6957.
38 F. Richter, M. Hochlaf, P. Rosmus, F. Gatti and H. D. Meyer, *J. Chem. Phys.*, 2004, **120**, 1306.
39 E. M. S. Maçôas, R. Fausto, J. Lundell, M. Pettersson, L. Khriachtchev and M. Räsänen, *J. Phys. Chem. A*, 2001, **105**, 3922.